ISSN 1063-7710, Acoustical Physics, 2019, Vol. 65, No. 2, pp. 216–225. © Pleiades Publishing, Ltd., 2019.

ACOUSTIC SIGNALS PROCESSING. COMPUTER SIMULATION

Mapping Microbubble and Ultrasound Spatio-temporal Interaction by M-mode Imaging: The Study of Feasibility[1]

R. Jurkonis[a], *, A. Sakalauskas[a], A. Lukoševičius[a], M. Maciulevičius[b], M. Tamošiūnas[b], and S. Šatkauskas [b]

[a] *Biomedical Engineering Institute, Kaunas University of Technology, Kaunas, LT-51423 Lithuania*

[b] *Biophysical research group, Vytautas Magnus University, Kaunas, LT-44404 Lithuania*

**e-mail: rytis.jurkonis@ktu.lt*

Received June 28, 2018; revised October 22, 2018; accepted October 30, 2018

Abstract—Ultrasound (US) and microbubble (MB) interaction is an important factor in the research of bioacoustics, as well as targeted drug and gene delivery. In this study, we demonstrate the feasibility of pulse–echo M-mode imaging system to be used for the visualization and quantification of US–MB interaction in both spatial and temporal dimensions. The system incorporates an exposure chamber with the cell–MB suspension, a 2.7 MHz focused US transducer, a US pulser–receiver and the customized LabView software. The results of cell and MB interaction obtained after M-mode image analysis have showed the US–MB interaction to be non-uniform in space and non-stationary in time. In order to quantify the spatio-temporal US–MB interaction, we have introduced the time function of spatial homogeneity dynamics. We have observed that the effective duration of interaction can be characterized at the predefined threshold of spatial homogeneity. For example, at the US excitation of 360 kPa peak negative pressure (15 bursts transmitted at 80 Hz pulse repetition frequency), the US–MB interaction persists for more than 5 seconds in the range at 4 mm depth of the exposure chamber with more than 50% of homogeneity. The system proposed in this assay is feasible for the characterization of US–MB interaction and can be exploited to optimize the MB concentration and/or the US excitation parameters.

Keywords: ultrasonic imaging, acoustical measurement methods in biological media

DOI: 10.1134/S1063771019020040

1. INTRODUCTION

Ultrasound (US) contrast agent microbubbles (MBs) facilitate the cell sonoporation [1–3]. A shear stress resulting from microstreaming [4] caused by linear MB oscillations (stable cavitation) induce a reversible cell membrane sonoporation. This can be exploited for targeted drug and gene delivery to cells and tissues as an alternative to biocompound intracellular transfer, associated to US thermal effects [5]. Nonlinear MB oscillations (inertial cavitation) occurring at high acoustic pressures can produce a jet phenomenon. Liquid jets induce more efficient cell membrane sonoporation, however they also pose direct harm to cells, reducing cell viability [6]. It has been shown by multiple studies that both stable and inertial cavitation can facilitate efficient drug and gene delivery [7].

As the mechanism of sonoporation is directly related to US and MB interaction, the variety of methods (B-mode imaging, Doppler imaging, passive cavitation detection, etc.) are developed for: i) the analysis of MB elastic oscillations [8], ii) the monitoring of MB activity [9], iii) MB concentration determination [10, 11], iv) the evaluation of MB dynamics [6, 12–15] and even v) the control of sonoporation efficiency [1, 16, 17]. The MB concentration in the medium can be evaluated using the optical microscope [18], however it is a time consuming task and does not allow online MB detection during the experiment. Another approach is to use the US B-mode diagnostic systems [11, 17, 19–21]. However, this method requires a separate electronic or mechanical scanning with a US beam, which makes the system complex and expensive. The presence of MBs in the medium can be also detected using passive cavitation detection systems, which comprise a separate broadband transducer receiving the acoustic emission signals for spectral content analysis [22, 23]. The passive acoustic detector was developed for the feedback process with the aim to achieve a controlled cavitation [24]. Based on the passive cavitation detection, several MB inertial cavitation dose metrics, such as inertial cavitation dose (ICD) [25], MB sonodestruction rate [26], the inverse of time to maximum value of spectral RMS [27] have been already proposed. Still, the intrinsic nature of MBs can lead to a relatively low delivery efficiency and large variation in bioeffect outcome [28–30].

[1] The article is published in the original.

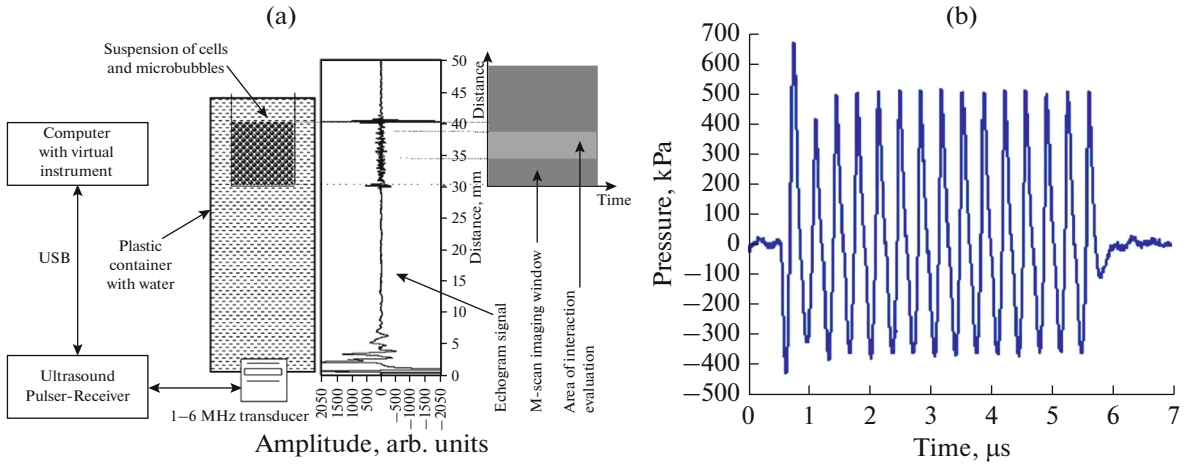

Fig. 1. The hardware setup designed for the imaging of US interaction with MBs in vitro. (a) The echogram from immersion container and exposure chamber is presented on the right side. Dotted lines indicate front part and top surface of the medium under investigation. The coordinates of the M-mode imaging are presented in relation to the position of the exposure chamber. The region of interest where the interaction was evaluated, is indicated in lighter grey color in M-mode. (b) Acoustic pulse waveform captured at the focal point of the beam (peak negative pressure P_n = 360 kPa, burst of 15 periods, space peak pulse average intensity is I_{sppa} = 5.8 W/cm^2, 80 Hz pulse repetition frequency, space peak time average intensity is I_{spta} = 34.7 mW/cm^2, pulse duration $\tau_{0.1}$ = 5 μs, acoustic working frequency $f_{3\text{dB}c}$ = 2.7 MHz).

To the best of our knowledge, US and MB interaction has not been simultaneously analyzed in the aspects of non-stationarity in time and non-uniformity in space. Thus, we considered the M-mode ultrasonic imaging to be a favorable tool for this analysis. A M-mode image consists of a series of echograms acquired at fixed time intervals. If US transducer is positioned on a sample, the stationary reflecting structure appears as the stationary pattern in the M-mode image. Conversely, if a scattering particle is in motion within the beam of the transducer, it appears as a moving pattern in the M-mode image. Previously it was reported that commercial MBs (5–10 μm) can be imaged using the standard M-mode equipment [31]. The M-mode was utilized to characterize US contrast agents by monitoring the translational effects of acoustic radiation force on each MB in a diluted population [32]. The feasibility of visual observation of the dynamics of the underwater medium by acoustic imaging was reported by Matveev et al. [33]. We hypothesized that the pulse–echo method that exploits a single transducer could be employed for the monitoring of US–MB interaction during sonoporation experiments. In this study, we investigate the feasibility to apply M-mode imaging method for the spatio-temporal characterization of cell and MB sample.

2. TECHNIQUES AND MATERIALS

2.1. Hardware Setup

A computerized US pulser–receiver system has been chosen for the implementation of M-mode imaging. The hardware system was equipped with drivers in order to develop LabView application for the hardware control. The setup structure is presented in Fig. 1.

The US transducer was spherically focused with a frequency band of 1–6 MHz, aperture diameter of 12 mm (model TS 12 PB 2-7 P30, Karl Deutsch Prufund Messgeratebau GmbH, Wuppertal, Germany). SonoVue MBs exhibit a maximum backscatter coefficient at around 3 MHz [34–37], which is close to the center frequency (2.7 MHz) of the chosen US transducer. It is worth mentioning that there are quite few trials to expand the US excitation frequency range below and above 1 MHz [1, 38–43]. The focal spot of the focused transducer beam determined in the pulse–echo mode was found to be at 33 mm from the transducer face. The beam was the narrowest (1.5 mm) at the focal spot. The acoustic pressure in the focal spot was measured with the needle hydrophone HNP-1000 (ONDA Corporation, Sunnyvale, CA, US), having a 1 mm active element. The hydrophone was coupled with an oscilloscope TDS-220 (Tektronix Inc., Beaverton, OR, US). The sensitivity of the hydrophone was corrected using the hydrophone capacitance C_h and acquisition channel (oscilloscope) input capacitance C_{in} = 20 pF. The final value of sensitivity at 2.7 MHz was M_c = 251 mV/MPa. The hydrophone manufacturer is declaring the calibration uncertainty ±1 dB for 1 V/mPa, which corresponds to ±12% for the pressures registered. The acoustic pressure waveform recorded at the focal spot of the beam is presented in Fig. 1b.

For the M-mode experiments, the exposure chamber was fixed at a focal distance of US transducer and kept stable during all tests. The exposure chamber was

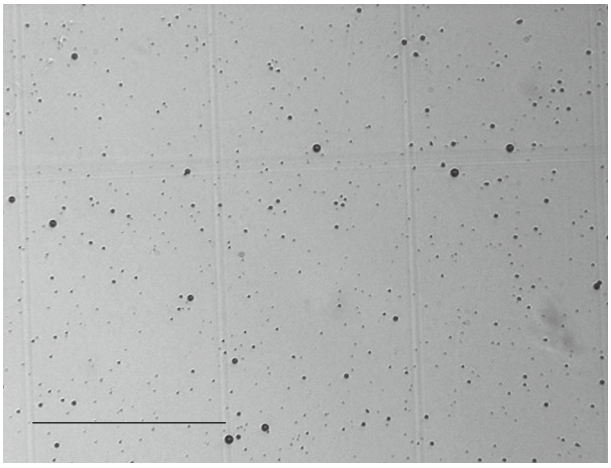

Fig. 2. Optical image of the representative microbubble sample. Scalebar 250 μm.

made from plastic tube with 5 mm inner and 7 mm outer diameter, respectively. 200 μl of sample suspension formed a column within the exposure chamber having a height of 10.2 mm. US waves were sent upwards into the exposure chamber positioned vertically. The top side of the exposure chamber was left open in order to access with the pipette tip. The bottom side of the exposure chamber was covered with the polyester membrane (thickness 28 μm), which was separating the suspension in the chamber from the immersion water. A polyester membrane is known to be transparent to sound waves [44]. The US transducer driven by a computerized US pulser–receiver USBox SX (Lecoeur Electronique, Chuelles, France) was excited with square shaped 175 ns duration voltage pulses of up to 270 V amplitude. The pulses were used for single pulse excitation and for the excitation bursts consisting of up to 20 periods. In all the cases, the pulse repetition frequency of excitation was 80 Hz. The receiver amplification was set to 30 dB, the filter was set to broadband (0.5 to 25 MHz) and the length of the acquired echogram was 70 μs or 52 mm. The analog-to-digital converter (ADC) had a 12 bits amplitude resolution and 80 MHz sampling frequency. A pulse–echo operation mode of the computerized US pulser–receiver was used in all the experiments.

The influence of a polyester membrane on the US transmission was verified with the same HNP-1000 hydrophone. When the membrane was inserted in the source beam, the acoustic peak negative pressure at the focal point was measured. After the comparison of acoustic pressures obtained in cases with/without membrane, the difference was found within the range of accuracy of oscilloscope (3%). All acoustic pressures were indicated through the entire paper mean peak negative pressures. The typical echogram from immersion container and exposure chamber is presented on the right side of Fig. 1a in relation with the dimensions of the setup.

2.2. Sample Preparation

The samples of suspension containing freshly prepared MBs and cells were investigated. Lipid-stabilized, air-containing MBs were produced by dissolving 1 mg of lyophilized powder containing macrogol 4000, distearoylphosphatidylcholine, dipalmitoylphos-phatidylglycerol sodium, and palmitic acid (Bracco S.A., Manno, Switzerland) in 200 μL 0.9% NaCl. The presence of MBs in the suspension was confirmed microscopically (Nikon Eclipse TS100, ×200)—Fig. 2.

Consequently, the MB concentration was determined by counting MBs using a hematocytometer, as described previously [26]. The counting of MBs was independently performed three times. The average MB concentration (estimated up to 2 min post MB preparation) was 6×10^7 MBs/mL. The stability of the prepared MB sample was time-dependent; the MB self-degradation followed the monoexponential decay curve with the time constant of 33 ± 4 min [17, 26]. In the experiment, all US data acquisition was performed within 10 min after preparation of the MB sample.

Next, the US–MB interaction experiments were performed on cell and MB suspension. The Chinese hamster ovary cells at 10^6/mL concentration were resuspended in 1× phosphate-buffered saline. The exposure chamber was pipette filled with uniform suspension of cells and MBs. The 200 μL of cell–MB suspension contained 1.6×10^5 cells and 1.2×10^6 MBs. Considering the US speed in the medium $c = 1480$ m/s, the delay of echo pulses in the column is 13.8 μs.

3. PROPOSED ANALYSIS OF ECHOGRAMS

The analysis of echograms was performed off-line using a developed LabView virtual instrument. The stored echograms were loaded from files as radio frequency signals (Fig. 3). Echo pulses from the suspension forepart (polyester membrane) and top surface (limited by air) were identified in the echogram. This allowed to demonstrate the temporal dynamics of the echogram signals reflected from cell and MB suspension in the exposure chamber.

The time window can be clearly seen in Fig. 3d, where the bottom covering membrane and the top surface of the suspension in the exposure chamber correspond to pulses at 40 and 55 μs, respectively. The echograms from the suspension show changes in scattering. The amplitude of the echo pulse when entering the chamber at 40 μs is high due to strong backscattering from the MB suspension at the onset of US exposure (0.21 s) when all MBs are still intact (Fig. 3b). It was not possible to observe echo pulses from the top surface of the suspension corresponding to 55 μs, because all US waves were scattered by high amount of

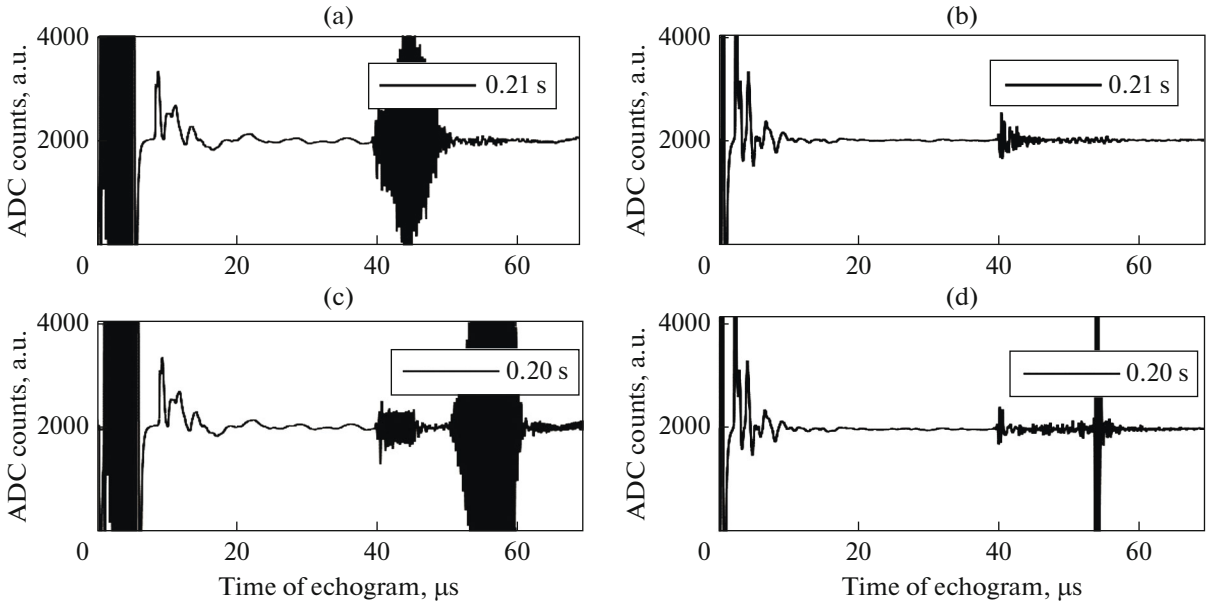

Fig. 3. Samples of the echograms showing MB dynamics in suspension after US excitation: (a) and (c) with 15-period burst of P_n = 360 kPa amplitude, (b) and (d) with a single pulse of P_n = 410 kPa amplitude. "0" on the *X*-axis denotes the time instance when the transducer is excited, the later (41–54 μs) fluctuation of amplitude represents echo pulses received from the exposure chamber. Time in the inset indicates the instance when echogram was received after the start of the exposure.

MBs (term "acoustic shadowing") in the forepart of the exposure chamber. The upper surface of MB suspension became evident in the echogram when MBs had been destroyed under the influence of intense US pulses during 20 s exposure (Fig. 3d). The absence of echo pulses at 54 μs (Fig. 3a) show that 15-period US burst pulses of 360 kPa for more than 0.21 s were unable to penetrate through the whole suspension with MBs. When MBs are gradually destroyed, US pulses pass the medium forth and back with a gradually decreasing loss of acoustic power. Finally, as MBs are destroyed during a 20 s excitation, the echo pulse from the top surface of the medium is clearly identified (Fig. 3c). Online interpretation of the echogram dynamics is complicated, implying a necessity of a new way to represent the ultrasonic data. Changes could be observed more clearly if the echograms were compared side-by-side during the time course. Thus, the M-mode imaging was used to visualize US interaction with cells and MBs in temporal and spatial dimensions (Fig. 4). The time dimension is directly related to US exposure duration, while the distance dimension can be intentionally set as respective windows in the echograms. Therefore, M-mode images were built from windowed echograms, as indicated in Fig. 1a. The time window was starting at 40.5 μs and terminating at 54.3 μs (Fig. 3d). We have also included additional 11.7 μs to involve MB post-excitation response into M-mode imaging window, which was reported [15, 45, 46] as a possible indicator of MB presence in the suspension.

In total, 370 echograms were acquired into computer memory during 20 s of excitation at 80 Hz pulse repetition frequency. Echograms were demodulated by calculating analytical signal after Hilbert transform and then taking the magnitude of the signal. Demodulated signals were filtered in order to remove the high-frequency noise. Then matrix of demodulated echographic data was presented as the intensity chart or M-mode image, where the amplitude of echograms is coded as the grayscale intensity. The grayscale intensity was adjusted to the amplitude of echo pulses from cell suspension: the highest amplitude was represented in black. This lower limit of grayscale was implemented to represent backscattered signals from the suspension with MBs as light gray–white pattern.

More detailed information on US interaction with cells and MBs was obtained in a specific region of the M-mode image, in the distance axis between 4.2 and 8.3 mm, which represents only the medium without stable reflection regions from bottom and top surfaces of the suspension (see Fig. 4a).

4. RESULTS

The proposed computerized US pulser–receiver system was first used to reveal the similarities and differences between M-mode images acquired from suspension of cells alone (Fig. 4a) and later from MB–cell suspension (Figs. 4b–4e). The cell–MB suspension was exposed to 360 kPa US excitation bursts consisting of up to 15 US pulses for 21 s (Figs. 4b–4d). When the number of US pulses was reduced to a single period,

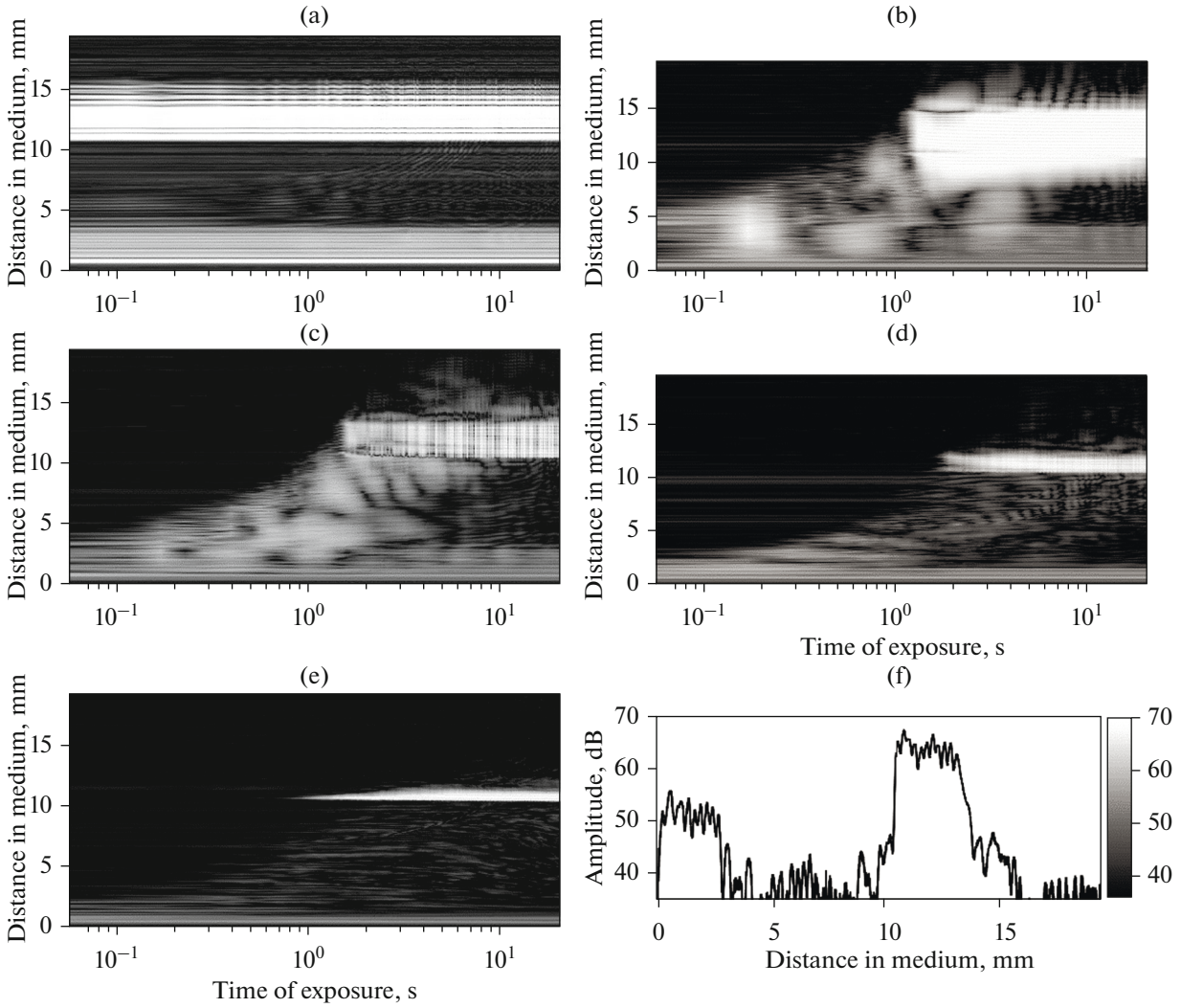

Fig. 4. M-mode images representing the dynamics of backscattered signal from the MB-cell suspension samples: (a) the suspension containing cells alone (9 minutes after pipetting), (b)–(e) dynamics of backscattered signal from cells suspension after MB administration. Cells–MBs suspension was excited with US: (b) 360 kPa, 15-period burst; (c) 360 kPa, 10-period burst; (d) 360 kPa, 5-period burst; (e) 410 kPa single pulse; (f) the profile of the magnitude of the backscattered signal from cell alone at the 20th second of exposure duration with adjusted grayscale. Black color was established at 46 dB level and was applied to all M-mode images.

the amplitude of this pulse was 410 kPa (Fig. 4e). M-mode images of the suspension represent the dynamics of the signal backscattered from the sample (10.2 mm) in the exposure chamber, including reflection from suspension–air interface and post-excitation region (above 10.2 mm). In order to magnify the beginning of the process, we prepared diagrams having logarithmic time axis.

The high-amplitude echo pulses from the interface at the bottom and top surfaces of the suspension appear as horizontal light patterns in all M-mode images. The first pattern is near 0 mm distance, the second, near 10 mm distance. The pattern thickness of the echo pulses, reflected from the entering interface of the suspension is directly related to the length of US excitation bursts. Therefore, the stationary pattern at the depths from 0 to 4 mm of the M-mode image is present in all the samples and is the first common feature of M-mode images. The depth range of this stationary pattern does not change during exposure duration. A stable high-reflectivity region with a thickness of about 4.2 mm can be seen in the case of the longest burst (15 periods) excitation (Fig. 4b). With a decrease of the number of US burst periods from 15 to 10, 5 and 1 period, the thickness of a stable strong reflection region decreased from 4.0 (Fig. 4b) to 2.9 (Fig. 4c), 1.5 (Fig. 4d) and 0.8 mm (Fig. 4e), respectively.

The second common feature of M-mode images observed in all the samples and in all the cases of US excitation is located at about 10.2 mm, where echo

pulses reflected from the top surface of the suspension form the second region of stable strong reflection. Again, the thickness of the pattern is directly related to the duration of US excitation bursts, but the time instance of a strong reflection depends on the type of sample in the chamber. If the suspension contains cells alone, then a strong reflection region is present and does not change in thickness during exposure duration. When the suspension is supplemented with MBs, a strong reflection region is not present at the very beginning of exposure and develops during 1–3 s of exposure, depending on the length of US excitation burst. The absence of strong reflection implies high attenuation or acoustic shadowing of MB suspension. This acoustic shadowing is gradually decreasing during US exposure duration and enables to detect the interface of high reflectivity from the top surface of the suspension.

After the identification of landmark patterns in M-mode images the analysis of US–MB interaction dynamics from cell–MB suspension samples was performed. The image region representing suspension is located between strong reflections—the bottom and top surfaces of the suspension. It can be seen in Fig. 4a that M-mode images of cell suspension do not change much during US exposure (in the distance range from 3.5 to 10.5 mm). The foremost finding in M-mode images of cell-only suspension is the minimal signatures of the static and moving scatterers in the suspension. The minimal light pattern shows that there are only weak scatterers in this suspension.

A characteristic feature of the M-mode images of the cell–MB suspension is a specific strong backscattering pattern (Figs. 4b–4e). It is also evident that during US exposure, the MBs are gradually fragmented with the US pulses and/or pushed-up from the analysis region due to acoustic radiation force, resulting in the decrease of the M-mode image intensity level from ~60 to ~40 dB compared to the cell-only sample. The non-uniformity of the intensity of M-mode images during the first 3 s of US exposure duration disclose the locations of high scattering and acoustic shadowing in the suspension. There are some locations containing cells as the main scatters, other locations—MBs and some zones of suspension—are in the acoustic shadow. For example (Fig. 4b), at the beginning of exposure the acoustic shadow extends from 7 mm to deeper regions corresponding to the upper suspension layer in the exposure chamber. This means that only the lower suspension layer (up to 7 mm), which is the nearest to the source transducer, is interacting with US during the very first series of US excitation. In case of a single pulse excitation, the region of initially non-affected suspension extends from 3 mm to deeper locations (Fig. 4e). Similarly, it implies that the suspension layer (up to 3 mm), the nearest to transducer, interacts with US during the very first excitation bursts. The time required for US to interact with the whole depth (10.2 mm) of suspension in the exposure chamber is related with the length of excitation bursts. US interacts with MBs in the whole suspension depth (10.2 mm) within 2 s in all the cases, except for a single 15-period US burst, where the time for interaction to spread is 0.7 s.

A detailed analysis of US interaction with MBs was performed within the region between 4.2 and 8.3 mm on the distance axis of M-mode image (Figs. 4b–4e). This distance range was chosen in order to exclude strong reflections from both the membrane and suspension top surface. The images show the US interaction with MBs to be non-homogeneous, having active and passive spatio-temporal zones, and last for different durations for different US excitation bursts. With the aim to estimate quantitatively the homogeneity of US–MB interaction, we introduced the threshold for M-mode image intensity. We set the threshold of M-mode magnitude to be at 46 dB as the highest amplitude observed in the medium containing cells alone (Fig. 4f). Consequently, in the presence of MBs the US–MB interaction is represented in white color in M-mode images. We counted the number of pixels in M-mode image region of higher intensity than 46 dB to get the quantity N_I associated with the locations of US–MB interaction. The rest pixels N_{NI} were estimated as the region without interaction. Thus, the US–MB interaction in space was quantitatively defined using the homogeneity parameter (recalculated to the percentage ratio) (1):

$$H = 100\% \frac{N_I}{N_I + N_{NI}}, \quad (1)$$

where $N_I + N_{NI}$ is the total number of pixels, which is equal to the length of the preselected window (distance range from 4.2 to 8.3 mm). This percentage ratio indicates the part of the active US–MB interaction in the analysis region. The homogeneity time function is obtained by calculating the H parameter at each instance of US excitation and represents the variation of US–MB interaction in a preselected depth range in the sample. The homogeneity time functions are presented in Fig. 5.

It can be observed that homogeneity fluctuations are more pronounced in the beginning of US exposure. Homogeneity increases during the first second of the exposure duration. After reaching around 100% homogeneity, the interaction does not decay monotonically. This can be explained by MB destruction and possible migration of non-destroyed MBs from the circumference of the exposure chamber into the region of acoustic beam. It is possible that a 1.5 mm width acoustic beam does not excite the total cross-section of the suspension in a tube with 5 mm inner diameter. When MBs initially located in the centre of the beam are destroyed, H temporarily decreases. Conversely, when MBs from the periphery of the beam move into the beam center, the homogeneity temporarily increases until these MBs are destroyed as well.

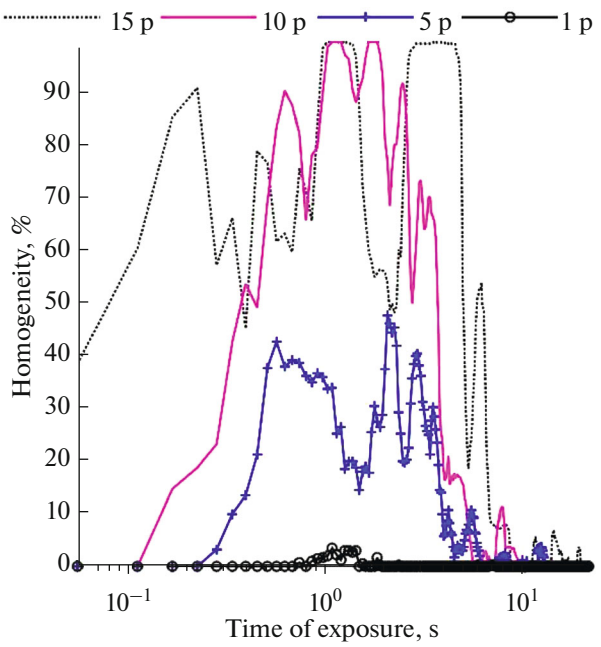

Fig. 5. Time dependence of homogeneity of US interaction with MBs calculated from M-mode images of intensity above 46 dB. In the legend number of periods in bursts of excitations is indicated, which peak negative pressure P_n = 360 kPa, only for the case of one-period burst – P_n = 410 kPa.

By applying the homogeneity parameter, we have estimated US–MB interaction for US excitation bursts having different number of periods. For example, the interaction persists more than 5 s in the depth range from 4.2 to 8.3 mm with more than 50% of homogeneity when US excitation is 15 periods in the burst (see Fig. 5). Considering the homogeneity level above 20% within the same 15-period excitation, the interaction persists for 6.5 s at the same depth. It is possible to achieve 3% of homogeneity for 11.8 s within the same US exposure. In the case of this 15-period US excitation more than 20% of suspension is in acoustic shadow for 0.15 s, therefore, no US–MB interaction occurs. The homogeneity levels of US–MB interaction and acoustic shadowing for different US excitations are summarized in the Table 1.

The second parameter characterizing the MB suspension is the time required for US waves to propagate through the medium. In the control case, when the suspension had cells alone, we observed high stable amplitude of the reflected waves from the top of the media at the distance of 11 mm. The amplitude at a 11 mm distance did not alter during the time of exposure (Fig. 4a). When the MBs were added, the high amplitude at 11 mm was observed with a delay (Figs. 4b–4e). We have evaluated this delay in detail using the amplitude threshold of 46 dB. The delay is the shortest (1.2 s) for the longest excitation burst (360 kPa, 15 periods), and increases as the excitation bursts become shorter. The numerical values are given in the Table 1.

In the Table 1 we can see that the time of US–MB interaction is becoming shorter at all spatial homogeneity levels with the decrease in the number of periods in the US excitation bursts. It can be observed that in response to the shortening of US excitation bursts from 15 periods to a single pulse the time duration when suspension with MBs is in the acoustic shadow increases from 1.2 up to 2.2 s. Respectively, the parameter of non-homogeneity or shadowing can be calculated as 100%—H. The latter evaluates the non-uniformity level of the US–MB interaction, as it is the opposite of the homogeneity parameter. This percentage indicates the extent of MB suspension (along the US propagation direction) being in the shadow and, therefore, unaffected by US.

5. DISCUSSION

The M-mode image represents the dynamics of US scatterers in the spatio-temporal dimension. The characterization of non-stationary processes in the suspension containing MBs during targeted molecular delivery experiments is the new application of the M-mode method. In this study US pulser–receiver system was used to excite MBs in the suspension and to compose the image from the echo pulses backscattered from the MBs. The pulser–receiver system in this approach was evaluated to be an economical tool for the investigation of US–MB interaction, as well as determined to be feasible for the current purpose. The M-mode image having time dimension is superior to

Table 1. Summary of parameters describing US interaction with MB in vitro

Number of periods in excitation burst	Peak negative pressure, kPa	Time of $H > 50\%$ homogeneity, s	Time of $H > 20\%$ homogeneity, s	Time of $H > 3\%$ homogeneity, s	Time to propagate the medium, estimated at 11 mm, s
15	360	5.3	6.5	16.7	1.2
10	360	3.2	4.5	7.2	2.1
5	360	0	2.9	6.8	2.3
1	410	0	0	0.06	2.2

the B-mode image if the imaging of non-stationary suspension is considered.

By investigating US–MB interaction, we assumed that the intensity of the M-mode images refers to the suspension echogenicity or backscattering strength, which is correlated to MB concentration [47]. A similar simplified model of MB suspension was employed by Nyborg, who described MB destruction [48]. The model for experiments has been verified by optical observations [47]. It has been shown that backscattering of a volume of all MB scatterers is proportional to the backscattered power from a single MB [46]. This implies that M-mode imaging can be used for the investigation of US–MB interaction kinetics in vitro. Furthermore, we have demonstrated for the first time that the US–MB interaction could be evaluated in the distance and time dimensions. Presented M-mode images show that US interaction with MBs in suspension does not start immediately in the whole exposure chamber with the very first bursts of US excitation. The interaction initially takes place at the forepart of the suspension facing US excitation transducer. The US pulses propagate into deeper layers of the suspension gradually destroying initially excited MBs. US waves propagate through the suspension with strong scattering due to MBs, therefore, the homogeneity of interaction depends on US intensity and MB concentration in situ. In all cases, the deepest layers of suspension with MBs are in the acoustic shadow, where the US–MB interaction is delayed. This indicates that at the fixed duration of US exposure, the deeper layers of MB suspension (both in the absence or in presence of the cells) can remain partially or completely unaffected by US.

This non-homogenous interaction can be taken into account for the explanation of high variability in the efficiency of sonoporation outcome [30]. Special attention must be paid here to molecular sonotransfer efficiency optimization. If the US parameters and MB concentration are adjusted to the pattern leading to the most part of MBs being in the shadow, then only a small part of the MB population will cavitate and temporarily permeabilize only the small number of cells. Eventually, the combination of these conditions leads to low molecular sonotransfer. On the other hand, high level of homogenous interaction may contribute to higher sonoporation efficiency. Thus, the quantification of homogenous spatio-temporal US–MB interaction could be proposed for molecular sonotransfer efficiency optimization by adjusting US output parameters to the MB concentration. Moreover, it is desirable to achieve high homogeneity during the onset of sonoporation and terminate the US excitation as homogeneity decreases to zero, thus avoiding cell death due to excessive impact of the US alone after complete MB sonodestruction had already occurred.

Recently our group has published research where MB cavitation extent quantified as spectral RMS was evaluated simultaneously with MB concentration measurements [27]. Spectral data showed that RMS rising phase appeared with some delay, while MB concentration decrease had been occurring since the onset of the US exposure. In addition to this, the latter MB concentration and RMS delay was decreasing with increasing acoustic pressure. The homogeneity of interaction and shadowing kinetics could facilitate the interpretation of the delay between MB concentration decrease and RMS increase. If the homogeneity of interaction is small and the major part of MBs is in the shadow, only the small portion of MBs undergoes inertial cavitation. Thus, MB concentration is decreasing, but there is no spectral RMS increase, because the remaining major part of MBs is obstructing the signal. Therefore, M-mode imaging facilitates the interpretation of spectral RMS and MB concentration decrease delay phenomena.

Our proposed M-mode mapping of US–MB interaction non-uniformity in space and non-stationarity in time could be compared with a number of similar experimental investigations. Sonovue MBs were excited [13] with US bursts of 10 cycles sine of 3.3 MHz. Total therapy sequence consisted of 100 pulses with repetition frequency of 10 Hz. The approximate MB concentration was 1.5×10^7 MBs/mL. The researchers found the exponential decay of backscattered subharmonic power and calculated the exponential time constant. The time constant was decreasing from 6 to 3 s when peak negative pressure was increased from 150 to 760 kPa. Our findings about US interaction with MBs are extracted from the total backscattered signal without selective spectra evaluation. However, we found that time duration of the interaction continues up to 6 s, therefore, our findings are similar. The second relevant reference of Sonovue observation using the time-dependent US image intensity was obtained by Min et al. [49]. Cadence pulse sequencing mode of US imaging (Acuson Sequoia 512; Siemens Medical Solutions, Erlangen, German) was performed with 15 MHz US probe (Acuson 15L8) at MI = 0.4 (1.55 MPa). Sonovue MB suspension was periodically exposed for 2 min to continuous US field with 10 min recess, and then the changes of US image intensity were observed. The US image intensity of Sonovue was completely diminished to zero within 20 min. Our proposal of M-mode imaging with single mono-element transducer could be an economical solution still enabling to quantify interaction homogeneity and shadowing parameters.

The proposed system has some limitations. The first one is related to the resolution of M-mode imaging, which is hindered by the duration of US excitation bursts. As an example, the effective duration of US pulse "hides" the part of the suspension located near the polyester membrane. A coupling layer with known dimensions could overcome this resolution limitation of the system. The second limitation of the proposed method is related to the specific backscattering spectra

of MBs of different sizes. If the frequency of the transducer is in the frequency band of a weak backscattering from MBs, then weak echo pulses from MBs will be received. Obviously, the proposed tool should be equipped with US transducer of respective center frequency allowing the optimal backscattering of preferred MBs.

The third lack of the proposed system concerns the single parameter included in the analysis. In our investigation, only the amplitude of the echograms was analyzed. Because of this limitation it is difficult to discriminate whether scattering in the suspension is originated specifically only from MBs. The presented system can be effectively applied only for in vitro investigations at present. The specificity of MB imaging could be improved by using spectral content of the echogram for M-mode image formation [22, 50, 51].

The variability of the derived parameters (homogeneity, propagation time) was not investigated, and this is a limitation in the present study. Concerning the statistics of the provided experimental results, we want to note the complex problem of MB concentration measurements [52]. The trials of MB counting reproducibility showed that the number of concentration variability up to 22% is achieved with optical microscopy [48]. So, we think that optical microscopy with intrinsic variability around 20% is the major contributor to the variability of our experimental results. Despite this, the preliminary results have proven the feasibility of M-mode imaging method for the US–MB interaction determination. The experimental data accurately defines the observed effects known from the acoustic wave scattering theory. We showed that M-mode US pulser–receiver system could be utilized for fast imaging of MB sonodestruction dynamics.

In conclusion, the proposed economic system based on M-mode imaging allows the visualization of US interaction with MB suspension in time and distance dimensions.

ACKNOWLEDGMENTS

This work was supported by grant (MIP-034/2013) from the Research Council of Lithuania.

REFERENCES

1. R. Karshafian, P. D. Bevan, R. Williams, S. Samac, and P. N. Burns, Ultrasound Med. Biol. **35** (5), 847 (2009).
2. T. A. Tran, J. Y. Le Guennec, P. Bougnoux, F. Tranquart, and A. Bouakaz, IEEE Trans. Ultrason., Ferroelectr. Freq. Control **55** (1), 43 (2008).
3. W. G. Pitt, G. A. Husseini, and B. J. Staples, Expert Opin. Drug Delivery **1** (1), 37 (2004).
4. P. Marmottant and S. Hilgenfeldt, Nature **423**, 153 (2003).
5. A. A. Anosov, O. J. Nemcenko, J. A. Less, A. S. Kazanskij, and A. D. Mansfeld, Acoust. Phys. **61** (4), 535 (2015).
6. P. A. Prentice, D. McLean, A. Cuschieri, K. Dholakia, M. R. Prausnitz, and P. Campbell, Nat. Phys. **1**, 107 (2005).
7. C. C. Coussios and R. A. Roy, Annu. Rev. Fluid Mech. **40**, 395 (2008).
8. V. M. Polunin, I. A. Shabanova, G. V. Karpova, N. S. Kobelev, K. S. Ryabtsev, V. B. Platonov, and I. M. Arefev, Acoust. Phys. **61** (4), 416 (2015)
9. T. Li, T. D. Khokhlova, O. A. Sapozhnikov, M. O'Donnell, and J. H. Hwang, IEEE Trans. Ultrason., Ferroelectr. Freq. Control **61** (10), 1698 (2014).
10. B. C. Tran, J. Seo, T. L. Hall, J. B. Fowlkes, and C. A. Cain, IEEE Trans. Ultrason., Ferroelectr. Freq. Control **52** (7), 1121 (2005).
11. C. Sciallero, M. Crocco, and A. Trucco, Meas. Sci. Technol. **22**, 1 (2011).
12. C. D. Ohl, M. Arora, R. Ikink, N. de Jong, M. Versluis, M. Delius, and D. Lohse, Biophys. J. **91**, 4285 (2006).
13. K. Hensel, M. Siepmann, A. Maghnouj, S. Hahn, and G. Schmitz, in *Proc IEEE Int. Ultrasonics Symposium* (Beijing, 2008), p. 1671.
14. Yu. N. Makov, Acoust. Phys. **55** (4–5), 536 (2009).
15. M. D. Santin, D. A. King, J. Foiret, A. Haak, W. D. O'Brien, Jr., and S. L. Bridal, J. Acoust. Soc. Am. **127** (2), 1156 (2010).
16. J. Alter, Ch. A. Sennoga, D. M. Lopes, R. J. Eckersley, and D. J. Wells, Ultrasound Med. Biol. **35** (6), 976 (2009).
17. M. Tamosiunas, R. Jurkonis, L. M. Mir, A. Lukosevicius, M. S. Venslauskas, and S. Satkauskas, Technol. Cancer Res. Treat. **11** 4, 375 (2012).
18. C. A. Sennoga, V. Mahue, J. Loughran, J. Casey, J. M. Seddon, M. Tang, and R. J. Eckersley, Ultrasound Med. Biol. **36** (12), 2093 (2010).
19. S. H. Hung, Ch. K. Yeh, T. H. Tsai, T. Chen, and R. Ch. Chen, Ultrasound Med. Biol. **37** (6), 949 (2011).
20. M. Lampaskis and M. Averkiou, Ultrasound Med. Biol. **36** (2), 306 (2010).
21. A. V. Patil, J. J. Rychak, A. L. Klibanov, Jr., and A. Hossack, Mol. Imaging **10** (4), 238 (2011).
22. S. I. Madanshetty, R. A. Roy, and R. E. Apfel, J. Acoust. Soc. Am. **90** (3), 1515 (1991).
23. A. Y. Ammi, S. L. Bridal, J. Mamou, G. I. Wang, and W. D. O'Brien, Jr., Proc. – IEEE Ultrason. Symp. **297** (4), F1129–34 (2006).
24. A. Sabraoui, C. Inserra, B. Gilles, J. C. Béra, and J. L. Mestas, Ultrason. Sonochem. **18** (2), 589 (2011).
25. W. S. Chen, A. A. Brayman, T. J. Matula, and L. A. Crum, Ultrasound Med. Biol. **29** (5), 725 (2003).
26. M. Tamosiunas, R. Jurkonis, L. M. Mir, A. Lukosevicius, M. S. Venslauskas, and S. Satkauskas, J. Ultrasound Med. **31** (12), 1993 (2012).
27. M. Maciulevicius, M. Tamosiunas, R. Jurkonis, M. S. Venslauskas, and S. Satkauskas, Mol. Pharm. **12** (10), 3620 (2015).
28. Z. Fan, D. Chen, and C. X. Deng, Ultrasound Med. Biol. **40** (6), 1260 (2014).
29. Y. Zhou, K. Yang, J. Cui, J. Y. Ye, and C. X. Deng, J. Controlled Release **157** (1), 103 (2012).

30. Z. Fan, R. E. Kumon, and Ch. X. Deng, Ther. Delivery **5** (4), 467 (2014).
31. R. S. Meltzer, E. G. Tickner, and R. L. Popp, Ultrasound Med. Biol. **6** (3), 263 (1980).
32. H. J. Vos, F. Guidi, E. Boni, and P. Tortoli, IEEE Trans. Ultrason., Ferroelectr. Freq. Control **54** (7), 1333 (2007).
33. A. L. Matveev, V. V. Mityugov, and A. I. Potapov, Acoust. Phys. **47** (2), 202 (2001).
34. M. Schneider, Echocardiography **16** (7–2), 743 (1999).
35. J. M. Gorce, M. Arditi, and M. Schneider, Invest. Radiol. **35** (11), 661 (2000).
36. P. S. Sidhu, P. L. Allan, F. Cattin, D. O. Cosgrove, A. H. Davies, D. D. Do, S. Karakagil, J. Langholz, D. A. Legemate, A. Martegani, J. B. Llull, C. Pezzoli, and A. Spinazzi, Br. J. Radiol. **79**, 44 (2006).
37. N. de Jong, M. Emmer, A. van Wamel, and M. Versluis, Med. Biol. Eng. Comput. **47** (8), 861 (2009).
38. A. J. Sojahrood, R. Karshafian, and M. C. Kolios, AIP Conf. Proc. **1481**, 351 (2012).
39. H. Hosseinkhah and K. Hynynen, Phys. Med. Biol. **57** (3), 785 (2012).
40. E. Sassaroli and K. Hynynen, Phys. Med. Biol. **50** (22), 5293 (2005).
41. J. M. Escoffre, A. Novell, J. Piron, A. Zeghimi, A. Doinikov, and A. Bouakaz, IEEE Trans. Ultrason., Ferroelectr. Freq. Control **60** (1), 46 (2013).
42. D. H. Thomas, V. Sboros, M. Emmer, H. Vos, and N. de Jong, IEEE Trans. Ultrason., Ferroelectr. Freq. Control **60** (1), 105 (2013).
43. M. Afadzi, C. L. Davies, Y. H. Hansen, T. Johansen, O. K. Standal, R. Hansen, S. E. Masoy, E. A. Nilssen, and B. Angelsen, Ultrasound Med. Biol. **38** (3), 476 (2012).
44. L. B. Feril, Jr., T. Kondo, Q. L. Zhao, R. Ogawa, K. Tachibana, N. Kudo, S. Fujimoto, and S. Nakamura, Ultrasound Med. Biol. **29** (2), 331 (2003).
45. A. Y. Ammi, R. O. Cleveland, J. Mamou, G. I. Wang, S. L. Bridal, and W. D. O'Brien, Jr., IEEE Trans. Ultrason., Ferroelectr. Freq. Control **53** (1), 126 (2006).
46. D. A. King, M. J. Malloy, A. C. Roberts, A. Haak, C. C. Yoder, and W. D. O'Brien, Jr., J. Acoust. Soc. Am. **127** (6), 3449 (2010)
47. K. Hensel and G. Schmitz, in Proc. 2010 IEEE Int. Ultrasonics Symposium (San Diego, CA, 2010), p. 1700.
48. W. L. Nyborg, Ultrasound Med. Biol. **32** (10), 1557 (2006).
49. H. S. Min, E. Kang, H. Koo, J. Lee, K. Kim, R. W. Park, I. S. Kim, Y. Choi, I. C. Kwon, and M. Han, Biomaterials **33**, 936 (2012).
50. D. E. Goertz, E. Cherin, A. Needles, R. Karshafian, A. S. Brown, P. N. Burns, and F. S. Foster, IEEE Trans. Ultrason., Ferroelectr. Freq. Control **52** (1), 65 (2005).
51. A. D. Mansfel'd, G. P. Volkov, A. G. Sanin, and I. A. Vladimirov, Acoust. Phys. **56** (3), 290 (2010).
52. Ch. A. Sennoga, J. S. M. Yeh, J. Alter, E. Stride, P. Nihoyannopoulos, J. M. Seddon, D. O. Haskard, J. V. Hajnal, M. X. Tang, and R. J. Eckersley, Ultrasound Med. Biol. **38** (5), 834 (2012).